ES2025-156619

THERMALLY ENHANCED BOARD TO MITIGATE HOT SPOTS IN LARGE SCALE CONCENTRATED SOLAR RECEIVERS

Luke J. Venstrom* Peter T. Krenzke Alex Kagay

Department of Mechanical Engineering and Bioengineering Valparaiso University Valparaiso, Indiana 46383 Nathan Van Velson David-Paul Schulze Calin Tarau

Advanced Cooling Technologies, Inc. Lancaster, Pennsylvania 17601

ABSTRACT

In this study, we evaluate heat pipes as an approach to distribute concentrated solar process heat in a solar receiver application. Temperature distributions on two stainless steel boards (304SS) were measured when exposed to concentrated solar thermal input in the solar furnace located on the campus of Valparaiso University. On the back of one board, we welded heat pipes fabricated from square tube steel stock; we call this board a constant conductance heat pipe thermally enhanced board (CCHP-TEB). No modifications were made to the other steel board. The temperatures of the two boards were measured using K-type thermocouples and an Optris PI 1M thermal imaging camera. At the same nominal power input, 0.93 kW, the CCHP-TEB was shown to have lower, more uniform temperatures than the plain stainless steel board. The maximum temperature of the *CCHP-TEB was* 590°C, *compared to* 719°C *for the plain board.* To reach a maximum temperature on the CCHP-TEB comparable to that of the plain board, a much higher solar input of 1.57 kW was required.

INTRODUCTION

Concentrated solar energy remains a promising component of a robust suite of low-carbon sources of energy for the future economy. Today, it is mostly used to generate electricity, but it can also be used as a source of process heat in difficult-todecarbonize industrial processes, a largely overlooked application. Process heat is also needed to drive thermochemical reactions for long-duration energy storage [1] or the production of synthetic fuels [2], two additional promising applications. An intrinsic advantage of concentrated solar is that it integrates low-cost thermal energy storage so that plants can continue to provide energy even during prolonged periods of no sunlight, *e.g.*, at night. The ability to provide energy on demand adds value to the energy, enough to offset the higher relative upfront cost of concentrated solar in some cases.

Concentrated solar plants feature one of four possible optical configurations: the parabolic trough, linear Fresnel, power tower, or parabolic dish [3]. The parabolic trough and linear Fresnel configurations focus sunlight to a line, limiting the extent to which the sunlight is concentrated and thus also the temperature that can be achieved. These configurations are suitable for applications that require temperatures below 500°C. The power tower and parabolic dish configurations focus sunlight to a point, enabling higher concentrations and higher temperatures that can exceed 1000°C. The power tower has been chosen for next generation concentrated solar technology (Gen3) promising to operate at higher temperatures than ever before [4].

To increase the efficiency of concentrated solar plants, efforts have focused on increasing the average temperature at which the solar receiver operates. Doing so requires a corresponding increase in the extent at which sunlight is concentrated in order to maintain high absorption efficiency. In point focus configurations, fluxes can exceed 5 MW/m² near the center of the focal region. Additionally, the distribution of flux is non-

^{*}Corresponding author. Email: luke.venstrom@valpo.edu

uniform [5]. Non-uniform and high heat fluxes combine to pose a significant design challenge. They lead to large temperature gradients and local temperatures that exceed the design temperature of the solar receiver, referred to as "hot spots." Hot spots increase losses from thermal emission, increase rates of fatigue from thermal cycling, and can even lead to receiver failure. In an obstructed flow receiver with a chevron mesh used to heat sand, hot spots irreversibly damaged the chevron mesh structure designed to increase the tortuosity of the sand flow through the receiver. The mesh structures deformed and softened to the extent that sand stuck to the chevron and clogged the flow path, rendering the receiver inoperable [6]. Hot spots also plagued the internal rotating structures of the CR5 solar receiver designed to support thermochemical hydrogen production via a nonstoichiometric redox cycle with heat recuperation, ultimately leading to the failure of the rotating reactive structures [7]. Means to mitigate hot spots in solar receivers are thus desirable as an enabling technology.

One possible solution to hot spots is the use of high-temperature heat pipes. Heat pipes are two-phase heat transfer devices that move heat through the evaporation and condensation of a working fluid, typically an alkali metal for high temperatures (>200°C). Heat pipes are capable of mitigating hot spots because they have an effective thermal conductivity that exceeds that of even the most conductive materials like copper, making it possible to rapidly transfer energy away from a hot spot and lower its temperature.

In the present study, we demonstrate the ability of sodium heat pipes to mitigate hot spots in a concentrated solar receiver. In this application, the heat pipes play a supporting role. They are not the primary solar receiver but rather are strategically employed to prevent failure of critical receiver components, such as the solid components of obstructed flow falling particle receivers or the window of a solar cavity receiver. Sodium heat pipes have also been considered as the primary absorber of concentrated solar radiation in solar receivers. We refer the reader to a recent article by Ji *et. al.* [8] or the nearly decade of work conducted at Sandia National Laboratories summarized by Adkins *et. al.* [9] for examples of heat pipes employed as the primary absorbers of concentrated solar radiation.

To evaluate heat pipes as a tool for preventing hot spot formation in concentrated soar receivers, we conducted a comparative experiment. We measured the steady-state distribution of temperature on a flat piece of stainless steel subjected to high-flux concentrated solar radiation in a solar furnace with and without sodium heat pipes attached to the shaded side of the steel. The steel with the heat pipes attached we call a "constant conductance heat pipe thermally enhanced board" (CCHP-TEB). The results confirm the effectiveness of sodium heat pipes to rapidly transport energy away from the points of highest flux and prevent overheating of the steel.

For readers that may be less familiar with heat pipes, we first

provide a brief primer on their operation and on the properties of sodium as the working fluid of choice for the heat pipes in the present study. Following the primer, we describe our experimental approach and results. Readers familiar with sodium heat pipes may skip ahead without loss of continuity.

HEAT PIPE OPERATION

Heat pipes leverage phase change to unlock heat transfer rates not possible with even the most conductive materials. They consist of a sealed pipe that is evacuated and then charged with a working fluid. A basic heat pipe features an evaporator region, where heat input vaporizes the working fluid, and a condenser region where the working fluid releases latent heat as it condenses. When the condenser region is located above the evaporator, gravity returns the liquid working fluid to the evaporator. A wick may be included to aid the liquid return, especially if the return is hindered by gravity.

In addition to being highly conductive, heat pipes act as thermal transformers and, in some cases, as thermal diodes. Properly designed and configured, they can absorb concentrated solar energy at a high flux and discharge it a lower flux and prevent heat from transferring backwards through the pipe to be lost to the environment when the concentrated solar energy input is removed. Finally, heat pipes are passive devices with no active components so long as gravity or capillary forces in a wick are able to return the liquid to the evaporating region.

The active material in a heat pipe may be a liquid or solid at room temperature. As heat is supplied to the evaporator and the evaporator region warms, the heat pipes eventually reach an activation temperature at which the vaporization, condensation, and transport of the working material are fast enough to sustain rapid rates of energy transfer between the evaporator and condenser regions. Once activated, the temperature differences between the evaporator and condenser regions become small and the pipes operate isothermally. Heat pipe activation is possible even when the vapor pressure of the working fluid is low, *e.g.*, below atmospheric pressure. An experimental study by Ma *et. al.* suggests that the activation temperature depends on heat pipe orientation [10].

Sodium was chosen for the heat pipes in the present study because its thermodynamic behavior aligns with the temperatures anticipated in high-temperature concentrated solar receivers. The expected operating temperatures fall between sodium's triple point of 371°C and its critical point of 2300°C. The correlation given by eqn. 1, plotted in Fig. 1 for reference, was recommended by Fink and Leibowitz [11] for sodium vapor pressure for temperatures from 590°C to 2090°C.

$$\ln P = 11.2916 \pm 0.5077 - (12532.694 \pm 87.141) / T - (0.3869 \pm 0.0600) \ln T \quad (1)$$

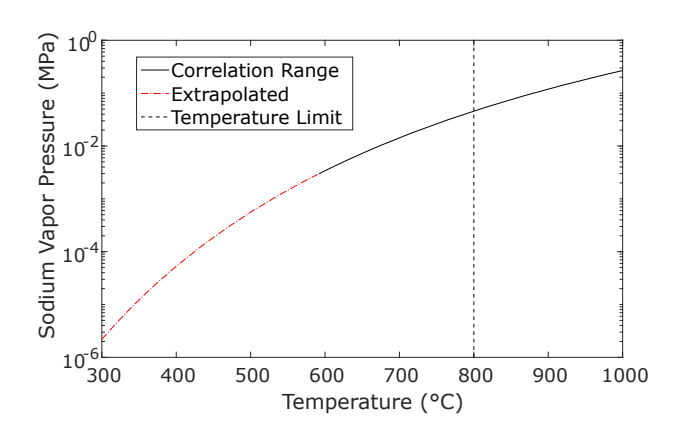


FIGURE 1. THE VAPOR PRESSURE OF SODIUM ACCORDING TO REF. [11]. THE VERTICAL LINE INDICATES THE UPPER TEMPERATURE LIMIT CHOSEN FOR OPERATING THE HEAT PIPES IN THE PRESENT STUDY, FOR WHICH THE VAPOR PRESSURE IS 0.056 MPA

EXPERIMENTAL METHODOLOGY

On-sun testing of the constant conductance heat pipe thermally enhanced board (CCHP-TEB) was completed at Valparaiso University's solar furnace facility [12] during March 2024. The solar furnace features an on-axis optical configuration with a faceted concentrator composed of 303 hexagon shaped mirrors arranged in a spherical array. The solar furnace is nominally able to supply a power of 5 kW over a 6 cm diameter focal spot, corresponding to mean solar fluxes of up to 1.77 MW m⁻². A motorized set of louvers regulates the amount of sunlight entering the concentrator of the furnace and, thus, the power of the concentrated sunlight delivered to the solar receiver.

The relative performance of the heat pipes was assessed by comparing temperature distributions of the CCHP-TEB to those of a plain 304 stainless steel (304SS) board of the same dimensions under nominally identical concentrated solar power. A power level of 0.93 kW was applied for the comparative testing during the experimental campaign. A second, higher power level of 1.57 kW was also applied to demonstrate peak performance of the heat pipes. In the following sections, we describe the CCHP-TEB and 304SS boards, the concomitant approaches employed to measure temperatures, and the two methods used to measure the power and intensity of the concentrated solar radiation incident on the boards during testing.

Thermally Enhanced Board and Experiment Set-up

The CCHP-TEB and plain stainless steel board were each mounted in the focal plane of the solar furnace behind a 50 mm thick section of Microtherm Promalight 1000X insulation as shown in Fig. 2. A 60 mm diameter aperture was cut into the insulation, allowing direct irradiation of the central portion of each

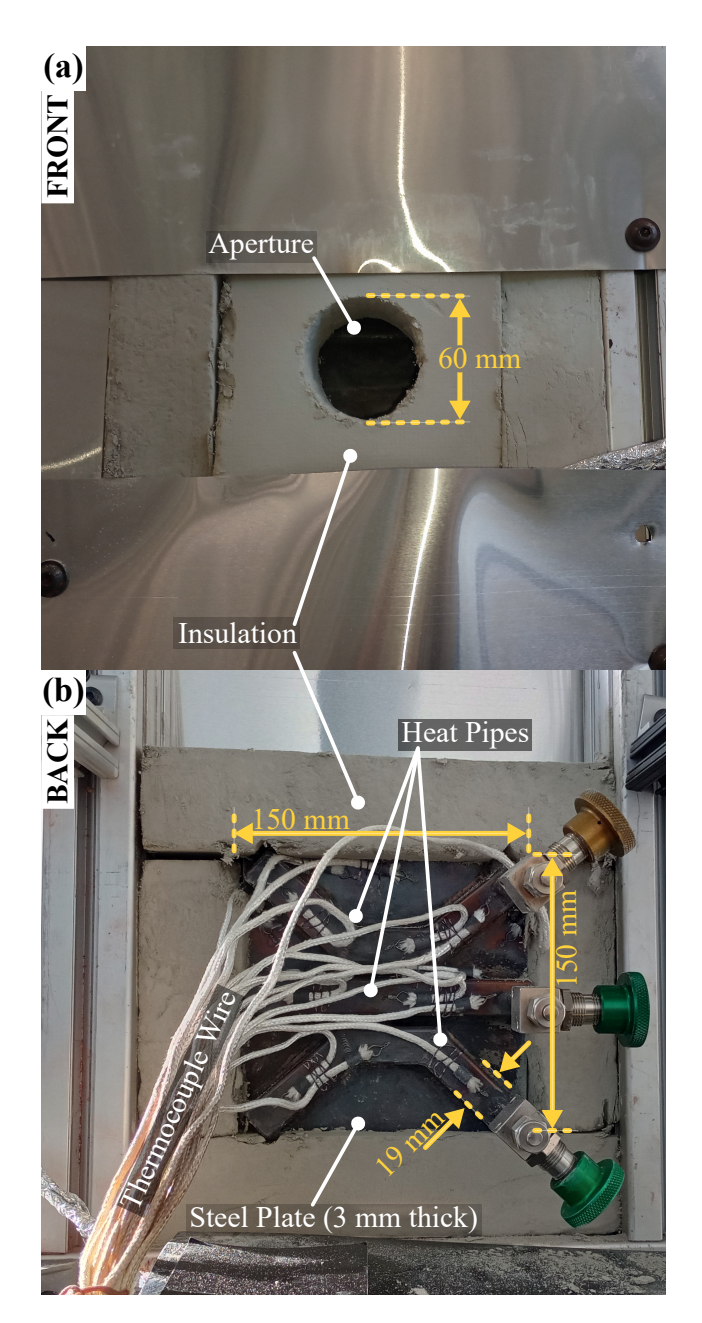


FIGURE 2. THE CONFIGURATION OF THE CCHP-TEB AND INSULATION ON THE TEST STAND AS VIEWED FROM THE (A) FRONT AND (B) BACK.

board by the high-flux solar radiation from the furnace. Additional insulation was placed around the edges of the boards and grooves were cut into the insulation 4-8 mm deep to hold the boards in place. The low thermal conductivity of the insulation, $<0.040~W~m^{-1}~K^{-1},$ minimizes heat transfer from the edges and front face of the board (except for the aperture) to the extent that these faces can be considered adiabatic. Solar thermal energy



FIGURE 3. BACK SIDE OF THE CCHP-TEB PRIOR TO TESTING.

absorbed by the boards is ultimately transferred to the surroundings via thermal radiation and convection through the aperture and from the back side of the board.

The dimensions of the CCHP-TEB and plain steel board are provided in Figs. 2 and 4. Both boards are 150 mm wide, 150 mm tall, and 3 mm thick and both are made from 304 stainless steel. The difference between the two boards is the addition of three square, sodium heat pipes attached to the back of the thermally enhanced board. The heat pipes have side lengths of 19 mm, 1.9-mm-thick walls, and are also made from 304 stainless steel. The evaporator sections of the heat pipes are located in the center of the board (positions 2, 5, and 6 in Fig. 4) such that they fall within the 6-cm-diameter irradiated region. The condenser sections of the central heat pipe are located outside of the irradiated region on the same horizontal plane as the evaporator section (positions 9 and 10). The condenser sections of the upper heat pipe are located above the evaporator section (positions 12) and 14) such that the return of condensed sodium to the evaporator is gravity assisted. The condenser sections of the lower heat pipe are located below the evaporator section (positions 3 and 11). With this arrangement, the condensed sodium must flow \approx 50 mm against gravity to return to the evaporator. This flow is achieved via capillary forces in a stainless steel wick located against the inner walls of the heat pipe.

As shown in Fig. 3, the square tubing that comprises the embedded heat pipe envelopes was welded to the back face of the stainless steel board, along with the end faces. For the top and bottom heat pipes, multiple sections of tubing were welded together. Fill tubes with valves were welded to each heat pipe to enable evacuation of the heat pipe volume and for charging with sodium working fluid. The heat pipes were leak checked to ensure hermeticity before sodium was charged into volume. All non-condensable gas was removed from the tubes prior to

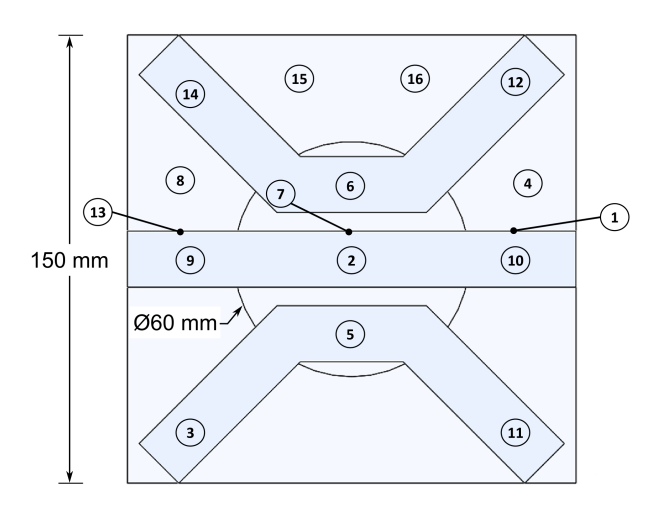


FIGURE 4. BACK VIEW OF THE CCHP-TEB HIGHLIGHTING THE LOCATIONS OF THE K-TYPE THERMOCOUPLES. THE CIRCLE ILLUSTRATES THE REGION ON THE FRONT OF THE BOARDS EXPOSED TO CONCENTRATED SOLAR RADIATION.

being charged with sodium. The heat pipes are thus considered to be "constant conductance". Had non-condensable gas been left in the pipes, they would have featured a variable conductance depending on the operating pressure.

Measurement of Temperature

The temperature distributions of the CCHP-TEB and the stainless steel board were measured with 16 K-type thermocouples spot welded to the back of the boards at the locations indicated by the numbers in Fig. 4. The junctions were positioned using a template to within 3 mm so that the measured temperatures on the boards are directly comparable at each numbered location.

The temperature distributions of the boards were also measured using an Optris PI 1M thermal camera positioned to view the back of the boards. The thermal camera provides a concomitant check on the contact measurements of the thermocouples. It also provides a more complete characterization of the temperature distribution since it establishes the temperature everywhere within its field of view rather than at discrete locations. The accuracy of temperatures indicated by the thermal camera is limited by the uncertainty in the thermal emissivity of the stainless steel surfaces of the boards. The emissivity depends on the oxidation of the surface. We assume $\varepsilon = 1$ for the wavelength region near 1 μ m within which the thermal camera operates. This assumption is reasonable for oxidized stainless steel. The plain 304SS board was unoxidized prior to testing, but was observed to be thoroughly oxidized following the experiment. The CCHP-TEB began its on-sun testing already oxidized from the charging process.



FIGURE 5. SOLAR CALORIMETER TO MEASURE THE SOLAR POWER DELIVERED TO A 6 CM CIRCULAR APERTURE.

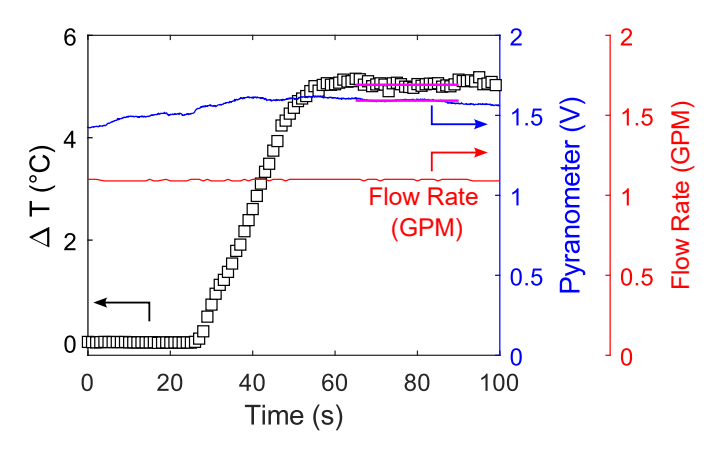


FIGURE 6. CALORIMETER ΔT AND PYRANOMETER OUTPUT WITH LOUVERS AT THE 60% SETTING AND A SOLAR POWER LEVEL OF 0.93 KW.

Measurement of Solar Power

The power delivered to the receiver aperture is quantified using two methods. In the first, a water-cooled calorimeter is employed. The second method utilizes an imaging technique to measure the distribution of heat flux delivered to the focal plane.

Solar Input: Calorimeter Method The calorimeter is shown in Figure 5. It is designed to minimize heat loss via reflection and emission of radiation from the calorimeter cavity, via conduction through the calorimeter walls, and via convection out of the cavity aperture. Consequently, the heat loss is negligible

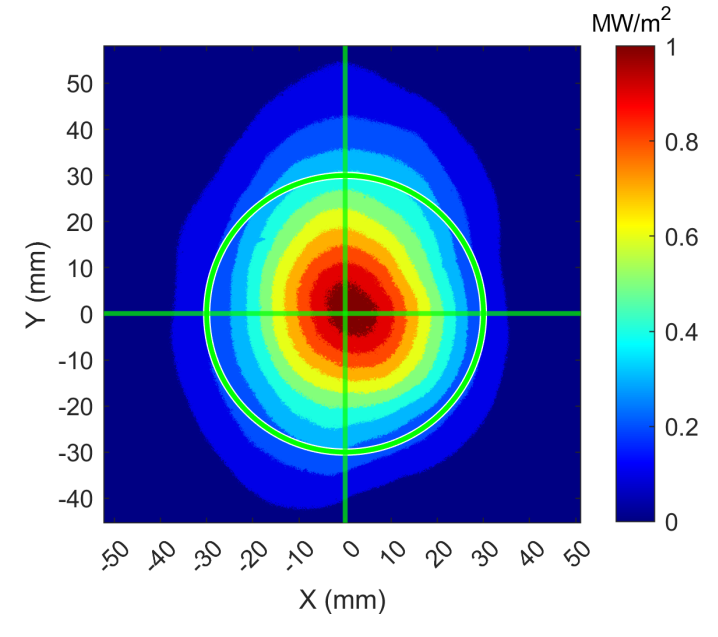


FIGURE 7. DISTRIBUTION OF FLUX IN THE FOCAL PLANE AT A CONCENTRATED SOLAR POWER LEVEL OF 1.57 KW

such that the calorimeter power is given by eqn 2.

$$\dot{Q}_{\text{calorimeter}} = \dot{m}C_p \Delta T \tag{2}$$

Experimentally, the flow rate of the water (m) is measured by a turbine flow meter, Vision BV2000-075, and the temperature rise of the water between the inlet and outlet (ΔT) is measured by a custom two junction thermopile constructed from two dual element thermocouple probes, Omega SCASS-062U-12-DUAL, and K-type thermocouple wire, Omega GG-K-24-SLE. The thermopile was calibrated against Pt-RTDs using two isothermal water baths over the temperature difference range from 0° C to 30° C. The specific heat capacity of the water (C_p) , assumed to be a constant, is established from the data published in Ref. [13] based on the average temperature of the water in the calorimeter $(T_{ave} = 0.5(T_{in} + T_{out}))$.

The solar input power is measured with the calorimeter at the same louver setting as was used when delivering the concentrated solar input to the CCHP-TEB. Because the available solar resource varies throughout the day due to sun position and atmospheric conditions, pyranometer readings are used to scale the calorimeter power measurements to determine the power delivered to the CCHP-TEB.

$$\dot{Q} = F_{\text{pyranometer}} \, \dot{Q}_{\text{calorimeter}} \tag{3}$$

The scaling factor, $F_{\text{pyranometer}}$, is defined as the ratio of the pyranometer output voltage during the experiment to its output during

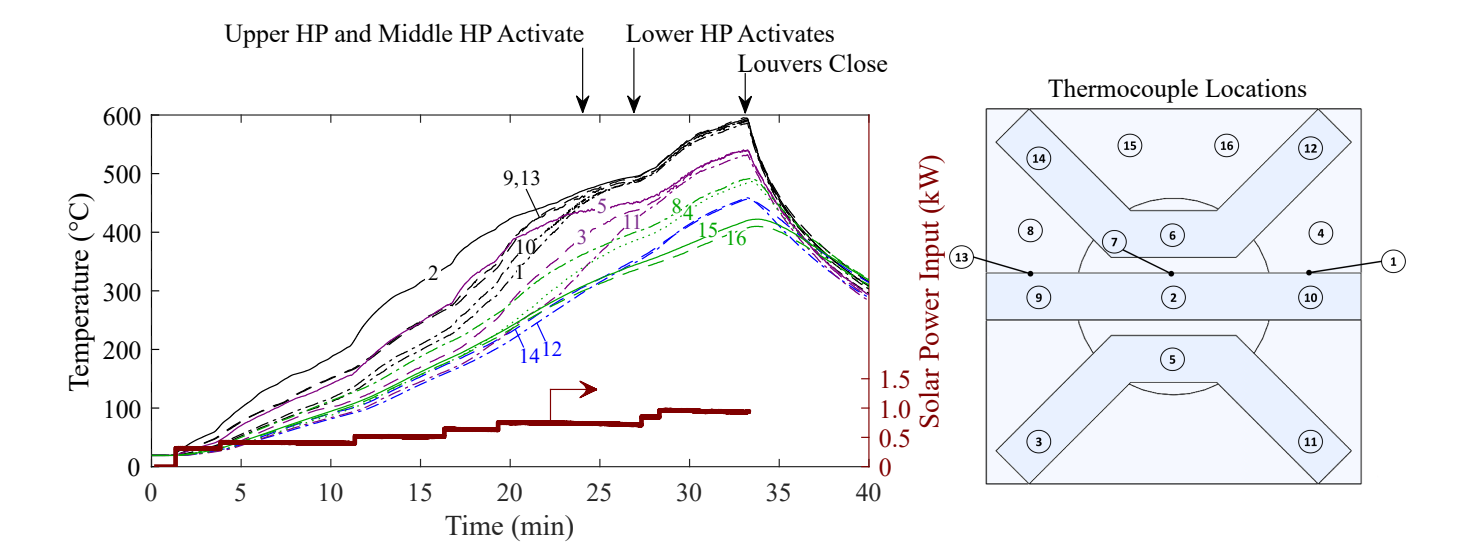


FIGURE 8. TEMPERATURES AND SOLAR POWER INPUT FOR THE CCHP-TEB IN AN EXEMPLARY EXPERIMENT WITH A MAXIMUM INPUT POWER OF 0.93 KW. NUMBERS INDICATE THERMOCOUPLE LOCATION AS PROVIDED IN THE CORRESPONDING DIAGRAM.

the calorimeter power measurement. The pyranometer, Apogee SP215, measures the global horizontal irradiation (GHI). On clear days, such as those when the testing was conducted, scaling of the GHI is a reasonable surrogate to scaling based on direct normal irradiance (DNI) measurements.

A calorimeter power measurement was completed for the CCHP-TEB test on March 13, 2024. The measured ΔT , pyranometer output, and flow rate are shown in Figure 6 with the solar furnace louvers at the 60% setting. The calorimeter ΔT stabilizes after 60 s. Quasi-steady operation is assumed after 65 s and the data is averaged between 65 s and 90 s to establish the values applied in eqn. 3 during the remainder of the experimental campaign in March. After averaging, the power was $\dot{Q}_{\text{calorimeter}}$ =1.46 kW with a pyranometer reading of 1.59 V and mass flow rate of \dot{m} =0.0693 kg s⁻¹.

Solar Input: Flux Maps Method Flux maps are acquired by reflecting the concentrated solar radiation at the focal plane into a camera. The radiation is diffusely reflected using a water-cooled Lambertian target. A Lucid Vision Atlas ATP204p camera is used to acquire a grayscale image of the light reflected from the target. The camera uses a Sony IMX541 monochrome image sensor outfitted with stacked neutral density filters, Midopt ND200 and ND300, and a fixed focal length lens, KOWA LM100FC24M.

The grayscale intensity varies proportionally with the incident power. Consequently, the flux at each pixel location is the product of the grayscale intensity and a proportionality constant.

The power within a region of an image is given by eq. 4

$$\dot{Q} = k \int_{A} GS \, dA \tag{4}$$

where GS is the grayscale intensity, dA is the pixel area, and k is the proportionality constant. The proportionality constant, k, was fixed by a point calibration against the calorimeter as the standard. With the calibrated k, the flux map approach of eq. 4 returns the same power within the 60 mm diameter aperture region of interest as the calorimeter measurement.

Flux maps were acquired within 20 minutes of completing temperature measurements and taking the boards off-sun in all experiments. Figure 7 shows the flux map acquired with the higher power level applied during the experimental campaign of 1.57 ± 0.24 kW. The direct normal irradiance was nominally steady at the time the flux map was acquired. The distribution of flux is approximately axisymmetric. Some asymmetry is expected due to optical errors in the solar furnace, especially pointing errors of the mirrors in the solar concentrator. The peak flux at the center of the aperture is near 1 MW m $^{-2}$. Similar fluxes might be expected at the aperture for a Gen3 central tower receiver.

RESULTS AND DISCUSSION

The results of an experiment conducted with the CCHP-TEB are provided in Fig. 8. They are exemplary of all experiments

conducted with the CCHP-TEB. Figure 8 shows the board temperatures measured by the thermocouples and the solar input power estimated from the pyranometer reading via eqn. 3 for the duration of the experiment. The solar input power is shown with a thick, red line, and temperatures are shown with thin lines. The thin lines are annotated with numbers to indicate the location of the thermocouples on the CCHP-TEB in reference to Fig. 4 (copied to the right side of Fig. 8 for convenience). The colors of the thin lines indicate which component of the CCHP-TEB the thermocouple was attached to. Black lines represent the temperatures indicated by thermocouples on the horizontal heat pipe in the center of the board (1, 2, 10, 9, and 13), blue lines represent the temperatures indicated by thermocouples on the upper, gravity-assisted heat pipe (12 and 14), purple lines represent the temperatures indicated by thermocouples on the lower heat pipe operating against gravity (3, 5, and 11), and green lines represent the temperatures indicated by thermocouples attached directly to the steel plate (4, 8, 15, and 16). Data is unavailable for thermocouples 6 and 7 due to a malfunction in the data acquisition system in this particular experiment.

Prior to the louvers opening when the solar input is 0 kW, all thermocouples read room temperature near 22°C. At t=2 min, the louvers are partially opened to establish a solar input power of 0.25 kW and the CCHP-TEB begins to heat up. During heat up and at all times that the CCHP-TEB was irradiated, the maximum temperature is observed at location 2 in the center of the board where the incident solar radiative flux is highest. Beginning at t=4 min, the louvers were progressively opened in small increments, slowly increasing the incident power level over the next 25 minutes to avoid overheating the board prior to the activation of the heat pipes. During this period, all heat pipes activated. The heat pipes are activated when the temperatures of the condenser and evaporator regions of the pipes collapse onto one another, indicating that the sodium vapor pressure has increased enough to sustain vapor flow through the center of the pipe from the evaporator to the condenser with a corresponding return flow of liquid at its walls.

It is easiest to see the activation of the lower heat pipe (purple lines: 3, 5, and 11) in the data of Fig. 8. At t=23 min, there is a large, >100°C difference in temperature between the evaporator (5) and the condensers (3 and 11). Between t=23 min and t=28 min, the difference rapidly disappears, and by t=30 min, the temperatures of the evaporator and condensers of the heat pipe are within 10°C. The heat pipe is nearly isothermal due to the steady evaporation and condensation of the sodium within the pipe. A similar behavior is also observed for the upper and middle heat pipes, but approximately 4 minutes before the activation of the lower heat pipe.

After the heat pipes activated, the concentrated solar input was increased to 0.93 kW, matching the power level input to the plain 304SS board, and was maintained for an additional 5 minutes. During this time, the CCHP-TEB continued to heat but

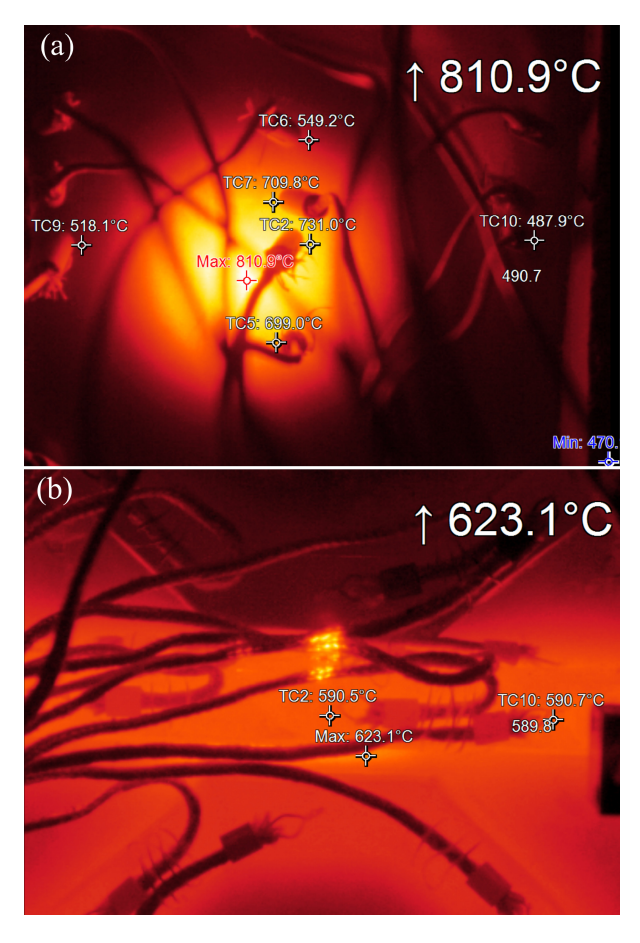


FIGURE 9. TEMPERATURE DISTRIBUTIONS MEASURED BY THE THERMAL CAMERA FOR (A) THE PLAIN 304SS BOARD AND (B) THE CCHP-TEB. BLACK WIRE OBSTRUCTIONS ARE THE INSULATED THERMOCOUPLE WIRES.

at a slower rate than during the activation period. The louvers closed at t=34 min, at which time the average rate at which the board was continuing to heat was \approx 10 °C /min. After the louvers closed, the CCHP-TEB cooled back to room temperature. In total, the CCHP-TEB was exposed to concentrated solar radiation for 32 minutes in this experiment. The thermocouples indicated a maximum temperature of 595°C on the central heat pipe at location 13 just before the louvers closed.

For the purposes of comparing the temperature measurements to those of the plain 304SS board, we averaged each temperature reading over the last minute of operation, just prior to the time when the louvers were closed. We now consider the distributions of temperatures measured on the two boards to evaluate the effectiveness of the CCHP-TEB at mitigating hot spots.

Figure 9 compares the temperature distributions of the CCHP-TEB and of the plain board measured with the thermal camera for the same level of incident power on the front of the

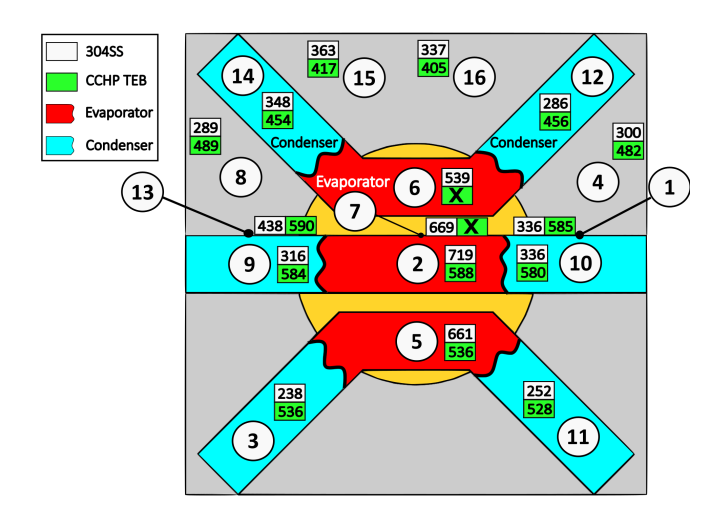


FIGURE 10. MEAN TEMPERATURES OF THE PLAIN 304SS BOARD (WHITE BOXES) AND CCHP-TEB (GREEN BOXES) IRRADIATED BY 0.93 KILOWATT.

boards, 0.93 kW. The figure also notes the maximum temperature in the field of view of the thermal camera in the upper right-hand corner of the images. Notably, the 623°C maximum temperature on the CCHP-TEB is 188°C lower than the 811°C maximum temperature on the plain board, a clear indicator that the CCHP-TEB more evenly distributes the concentrated solar energy absorbed than the plain board. The more uniform distribution of temperature in the CCHP-TEB is also evident when comparing the thermal images. In the image of the plain board (Fig. 9a), a circle is visible. This circle is the region in which the board is irradiated. Absorbed energy is not effectively transported away from this region of the plain board. In contrast, there is no comparable circle in the image of the CCHP-TEB (Fig. 9b) because the absorbed solar energy is more rapidly transferred away from the irradiated region through the heat pipes.

The thermocouple measurements corroborate the thermal camera measurements. The temperatures measured at each thermocouple location on the plain board and CCHP-TEB are overlaid on the thermocouple position diagram in Figure 10 for the 0.93 kW incident radiative power level on the plain 304SS board and CCHP-TEB, the same condition depicted in the thermal images of Fig. 9.

The temperatures are calculated as the average temperature over the last 1-minute of operation at the indicated power level. The thermocouples attached to the individual heat pipes indicate nearly isothermal conditions in the heat pipes while on-sun. For example, in the center heat pipe, the evaporator temperature is 588°C (position 2) and the condenser temperatures are 584°C (position 9) and 580°C (position 10), respectively. No more than a 10°C difference in temperature is observed in any of

the heat pipes with 0.93 kW power input. In contrast, on the plain 304SS board temperature differences across the same locations as those on the CCHP-TEB are as large as 423°C. Looking at the maximum temperature difference for all thermocouple locations, the plain 304SS board has variations of 480°C, compared to 185°C for the CCHP-TEB.

TABLE 1. MEAN TEMPERATURES OF THE 304SS BOARD AND CCHP-TEB INDICATED BY THERMOCOUPLES WITH 0.93 KW SOLAR INPUT AS WELL AS MEAN TEMPERATURES OF THE CCHP-TEB WITH 1.57 KW INPUT.

Location	Label (Fig. 4)	304SS Board (0.93 kW) (°C)	CCHP-TEB (0.93 kW) (°C)	(1.57 kW) (°C)
Top HP	6	539	NA	570
Top HP	12	286	456	587
Center HP	13	438	590	732
Center HP	7	669	NA	735
Center HP	1	336	585	725
Center HP	9	316	584	719
Center HP	2	719	588	724
Center HP	10	336	580	713
Lower HP	3	238	536	650
Lower HP	5	661	536	639
Lower HP	11	252	528	635
Plate	8	289	489	627
Plate	4	300	482	615
Plate	15	363	417	548
Plate	16	337	405	531

The improved heat transfer and temperature uniformity of the CCHP-TEB allowed an additional test with higher input power. The CCHP-TEB was heated in a similar manner as before, but reached a maximum input power of 1.57 kW, which was maintained for 16 minutes. After 12 minutes, temperatures peaked and then declined slightly due to small decrease in the solar input. The rate of temperature change for the last minute was less than 4°C/min at all thermocouple locations. Mean thermocouple temperatures for the same period are included in the last column of Table 1. The maximum temperature indicated by the Optris P1 1M thermal imaging camera was 813°C, similar to the maximum temperature indicated for the plain 304SS board. Despite 69% higher input power, the CCHP-TEB was able to maintain temperatures within the limit for operating with 304SS.

CONCLUSION

Hot spots represent a technical design challenge in concentrated solar energy receivers, particularly those in the power tower and parabolic dish optical configurations. In this study, we proposed the use of alkali metal heat pipes to mitigate hot spots due to their high effective thermal conductivity and passive operation so that solar receiver surfaces can be safely exposed to more intense incident fluxes than would otherwise be possible. The ability to mitigate hot spots is poised to become even more important as Gen3 solar receivers continue to push towards operating at higher temperatures and thus also higher concentrated solar radiative fluxes. To demonstrate the ability of heat pipes to mitigate hot spots, we developed a thermally enhanced steel board and tested it on-sun in the solar furnace located at Valparaiso University.

The relative performance of the heat pipes was assessed by comparing temperature distributions of an irradiated thermally enhanced board with constant conductance heat pipes (CCHP-TEB) to those of a plain 304 stainless steel board (304SS) of the same dimensions as the plate to which the CCHP thermal enhancement was applied. Under nominally identical operating conditions with a solar input power level of 0.93 kW, the CCHP-TEB was shown to lower peak temperatures by nearly 200°C compared to the plain 304SS board. The plain board reached a maximum temperature of 811°C whereas the peak temperature of the thermally enhanced board was 623°C.

A much higher solar input of 1.57 kW was required to heat the CCHP-TEB up to a comparable maximum temperature observed at a 0.93 kW solar input on the plain steel board. The thermally enhanced board thus shows promise as a means to mitigate hot spots when strategically employed at locations of maximum flux in solar receivers.

ACKNOWLEDGMENT

The authors thank the Department of Energy for the Small Business Innovation Research (SBIR) Phase I award (DE-SC0023832) that enabled this work. The authors would also like to thank the following students at Valparaiso University for their assistance during the on-sun testing in the solar furnace: Micah D'Arcangelo, Ethan Duff, Noah Fisher, Max Van Den Berg, Joshua Mangnall, and Mario Ramos. The authors would also like the thank the following ACT technicians for assistance in fabricating the CCHP-TEB: Sam Martzall and Phil Texter.

REFERENCES

[1] Bassett, K., Silcox, R., Will, J. D., Hill, S., Smith, P., Smith, B., Schmit, B., Venstrom, L. J., and Krenzke, P. T., 2024. "Fungible, multiyear solar thermochemical energy storage demonstrated via the cobalt oxide cycle". *Journal of Solar Energy Engineering*, 146(5), p. 051004.

- [2] Warren, K. J., and Weimer, A. W., 2022. "Solar thermochemical fuels: Present status and future prospects". *Solar Compass*, *1*, p. 100010.
- [3] Steinfeld, A., and Palumbo, R., 2001. "Solar thermochemical process technology". *Encyclopedia of Physical Science and Technology*, **15**(1), pp. 237–56.
- [4] Mehos, M., Turchi, C., Vidal, J., Wagner, M., Ma, Z., Ho, C., Kolb, W., Andraka, C., and Kruizenga, A., 2017. Concentrating solar power Gen3 demonstration roadmap. Tech. rep., National Renewable Energy Lab (NREL), Golden, CO (United States).
- [5] He, Y.-L., Wang, K., Qiu, Y., Du, B.-C., Liang, Q., and Du, S., 2019. "Review of the solar flux distribution in concentrated solar power: Non-uniform features, challenges, and solutions". Applied Thermal Engineering, 149, pp. 448– 474.
- [6] Saeed, R. S., Djajadiwinata, E., Alswaiyd, A., Alaqel, S., Saleh, N. S., Al-Ansary, H., El-Leathy, A., Jeter, S., Danish, S. N., Al-Suhaibani, Z., Sarfraz, M., and Almutairi, Z., 2023. "Material compatibility between discrete structures and candidate particulates in a particle heating receiver of a concentrated solar power system". AIP Conference Proceedings, 2815(1), 10, p. 020014.
- [7] Diver, R. B., Miller, J. E., Siegel, N. P., and Moss, T. A., 2010. "Testing of a CR5 solar thermochemical heat engine prototype". In ASME 2010 4th International Conference on Energy Sustainability, ES2010, Vol. 2, pp. 97–104.
- [8] Ji, Y., Yuan, D., Hao, Y., Tian, Z., Lou, J., and Wu, Y., 2022. "Experimental study on heat transfer performance of high temperature heat pipe with large length-diameter ratio for heat utilization of concentrated solar energy". *Applied Thermal Engineering*, 215, p. 118918.
- [9] Adkins, D. R., Andraka, C. E., Moreno, J. B., Rawlinson, K. S., Showalter, S. K., and Moss, T. A., 1999. "Heat pipe solar receiver development activities at Sandia National Laboratories". In Proceedings of the Renewable and Advanced Energy Conference for the 21st Century Conference.
- [10] Ma, Y., Yu, H., Huang, S., Zhang, Y., Liu, Y., Wang, C., Zhong, R., Chai, X., Zhu, C., and Wang, X., 2022. "Effect of inclination angle on the startup of a frozen sodium heat pipe". *Applied Thermal Engineering*, 201, p. 117625.
- [11] Fink, J. K., and Leibowitz, L., 1995. Thermodynamic and transport properties of sodium liquid and vapor. Tech. rep., Argonne National Laboratory (ANL), Argonne, IL (United States), 01.
- [12] Duncan, G. S., Nudehi, S., Palumbo, R., and Venstrom, L. J., 2014. "A high-flux solar furnace for undergraduate engineering education and high-temperature thermochemistry research". In ASME 2014 8th International Conference on Energy Sustainability, ES2014, collocated with the ASME 2014 12th International Conference on Fuel Cell

- Science, Engineering and Technology, Vol. 1, pp. 1–7.
- [13] Bergman, T. L., Lavine, A. S., Incropera, F. P., and DeWitt, D. P., 2017. Fundamentals of heat and mass transfer. John Wiley & Sons, Nashville, TN.